A Comparative Theoretical Study on DMABN: Significance of Excited State Optimized Geometries and Direct Comparison of Methodologies

Andreas B. J. Parusel,*,† Wolfgang Rettig,‡ and Wibke Sudholt§

Institute for Theoretical Chemistry and Structural Biology, University of Vienna, Rennweg 95b, 1030 Vienna, Austria, Institut für Chemie, Fach-Institut für Physikalische und Theoretische Chemie, Humboldt-Universität zu Berlin, Brook-Taylor-Strasse 2, 12489 Berlin, Germany, and Institute of Theoretical Chemistry, Heinrich-Heine-University, Universitätsstrasse 1, 40225 Düsseldorf, Germany

Received: July 21, 2001; In Final Form: November 5, 2001

Theoretical studies are presented for 4,-*N*,*N*-dimethylaminobenzonitrile (DMABN) by using the semiempirical Austin model 1 (AM1) and ab initio Hartree−Fock (HF) methodology for optimization of the electronic ground and AM1/configuration interaction with both single and double excitations (CISD) and HF/configuration interaction with single excitation (CIS) for the lowest excited states. For a correct description of the ground-state structure, additional polarization functions and at least a split-valence double-ζ basis set have to be used. For both the ground and excited states of DMABN, the relative orientation of the two methyl groups is important: AM1/CISD predicts both the first (^1L_b character) and second excited state (^1L_a character) to be of untwisted and slightly pyramidalized structure with the methyl groups oriented in a staggered conformation. HF/CIS computes the L_a state at lower energy than the L_b state in contrast to experimental data. This incorrect state ordering represents a serious problem for geometry optimization as only the lowest excited state of a given symmetry can be optimized because of root flipping. The HF/CIS L_a optimized geometry is twisted by about 30° yielding the methyl groups in an eclipsed conformation. Optimization of the twisted intramolecular charge-transfer state (TICT) yields different geometries for both methods. Both methods calculate the dimethylamino group for a 90°-fixed twist angle to be of sp^2-hybridization (i.e., without pyramidalization). The AM1/CISD-optimized structure, however, has a widened amino−carbon bond length and aromatic (nearly equal) benzene bonds, whereas the HF/CIS-optimized structure yields a shortened amino−carbon bond and alternating benzene bond lengths. The results of AM1/CISD, HF/CIS, complete active space self-consistent field (CASSCF), and second-order perturbation theory (CASPT2), time-dependent density functional theory (TDDFT), density functional theory/single-excitation configuration interaction (DFT/SCI) and multireference configuration interaction (DFT/MRCI) single-point calculations are compared by using both the AM1/CISD- and HF/CIS-optimized geometries for the calculation of absorption and emission energies. The results of both the CASPT2 and all DFT-based methods are in qualitatively good agreement with experimentally obtained absorption energies. A comparison of calculated emission energies by using excited-state geometries with data using ground-state optimized geometries shows the necessity to use optimized excited-state geometries for computation of emission energies. The first excited-state energy surface pathway corresponding to the photoreaction from the planar ^1L_b to the ^{1}TICT state can only be obtained with AM1/CISD geometries. A strongly endothermic reaction is predicted by AM1/CISD, HF/CIS, and CASSCF, a slightly exothermic reaction by CASPT2 and the DFT/configurations interaction methods, and a strongly exothermic reaction by the time-dependent DFT methodology. Experimentally, a slight increase in energy is found.

1. Introduction

Electron transfer (ET), charge transfer (CT), and energy transfer are fundamental steps in natural processes such as photosynthesis. Innumerable attempts have been made both by experimental and theoretical chemists to get a closer insight into the understanding of the exact mechanisms in these systems. Nevertheless, we are still far away from understanding these electron- and energy-transducing mechanisms for large and complex molecules. Methods of quantum chemistry have proven to be an important tool for investigation of these processes. Despite the progress in this field, it still is quite difficult to calculate ET or CT characteristics, i.e., properties of systems in their electronic excited states, even for relatively small molecular systems.[1] Many theoretical investigations have been conducted only for the electronic ground state. Comparably few calculations have been published for the excited states, and even fewer include changes in molecular structure upon excitation, i.e., optimization of excited-state geometries. However, several photophysical processes (e.g., fluorescence or electron transfer) should require the calculation of optimized excited-state geometries as significant conformational relaxations take place after photoexcitation. Much effort has been put into the development of methods for optimization of excited states, but only a few are available even for small organic systems with about 10 non-hydrogen atoms. Herein, the single-reference configuration interaction with single excitations (CIS)[2] method is still

* Corresponding author. E-mail: andreas.parusel@univie.ac.at.
† University of Vienna.
‡ Humboldt-Universität zu Berlin.
§ Heinrich-Heine-University.

10.1021/jp015513m CCC: $22.00
Published on Web 01/10/2002

frequently used. It allows the optimization of excited-state geometries of relatively large molecules. However, the calculated excited-state properties are often far from satisfactory, and calculated energies deviate significantly from experimental data; also, the order of the excited states is sometimes not reproduced correctly.[2,3] The complete active space self-consistent field (CASSCF)[4] method represents a further approach for geometry optimization of electronic excited states. It is able to account adequately for the important nondynamic electron correlation effects caused by nearly degenerated configurations. Also, this method suffers from a shortcoming: Only relatively few orbitals can be included in the complete molecular orbital (MO) active space. Problems thus arise when the active orbitals change during optimization of the geometry. The computational cost is also a serious problem, at least for larger systems. One promising approach to include the contribution of additional electron correlation is the combination of geometries optimized by the CASSCF method with a multiconfigurational complete active space second-order perturbation theory (CASPT2) approach.[5,6] The CASPT2 method is used to obtain corrections to the excitation energies, which are due to dynamic electron correlation effects, which often are of critical importance for obtaining quantitatively accurate results. The high computational cost restricts the size of the systems that can be calculated. Geometry optimizations are practically not possible at the moment. The limited number of active orbitals also excludes several problems with numerous active valence electrons to be treated by this method.

The combination of an analytical gradient method for excited-state geometries [Hartree−Fock (HF)/CIS or CASSCF, where possible] with a qualitatively high first-principle method for energy and electronic properties is a promising alternative for calculation of excited-state properties. Regrettably, these possibilities have been used only rarely in the literature. Apart from CASPT2, several further qualitatively high first-principle methods are available for calculation of excited-state properties. Density functional theory (DFT)-based methods have proven to give reliable results for ground-state properties even of relatively large systems with several hundreds of electrons. There has been significant progress in the extension of DFT-based methods for excited-state properties, namely the time-dependent density functional theory (TDDFT)[7,8] and a combination of DFT with single and multireference configuration interaction (DFT/SCI[9] and DFT/MRCI[10]). The DFT/SCI method is based on the single-excitation configuration interaction (SCI) approach with the configuration interaction (CI) Hamiltonian matrix elements modified and corrected empirically. Molecular orbital eigenvalues are taken from gradient-corrected Kohn−Sham DFT. In 1999, extension of this method toward a multireference CI was presented, where states of multiconfigurational character can also be described. Recently, excited-state gradients have also been implemented in DFT,[11] but much further investigation is required before the quantitative accuracy is assessed.

Not only the correct choice of a sophisticated method is crucial for a correct reproduction of experimental data, but also a sufficiently flexible basis set is often necessary. On the other hand, the combination of a large basis set with qualitatively low methods (e.g., HF/CIS/6-31++G**) is a somewhat questionable procedure. Basis sets are often chosen somewhat arbitrarily. Thus, a kind of guideline for the best basis set is quite important as this work will show. First-principle methods cannot be used for large systems with thousands of electrons. Here, semiempirical methods are still used widely for calculation of ground-state properties.[12] Intermediate neglect of differential overlap with spectroscopic parametrization (INDO/S and ZINDO/S from Zerner) semiempirical methods[13] have been parametrized particularly for reproduction of absorption spectra, i.e., computation of excited-state properties. It is also possible to optimize electronic excited states, although the Hamiltonians have not been parametrized for calculation of excited-state gradients. Nondynamic electron correlation is taken into account by a configuration interaction scheme, e.g., with both single and double excitations (CISD). For some methods, dynamic electron correlation is considered implicitly in the parametrization. The active space often can be extended up to 10 or even 20 orbitals. To get an idea about the reliability of semiempirical methods for excited-state calculations it is important to compare these results with those of expensive first-principle methods.

SCHEME 1

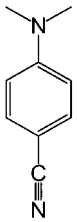

A variety of donor−acceptor molecules have been investigated in their excited states as they undergo charge or electron transfer. One class of these intramolecular charge-transfer systems shows dual fluorescence; the most well-known example is 4,-*N*,*N*-dimethylaminobenzonitrile (DMABN)[14] (see Scheme 1). Under jet-cooled conditions and in very apolar solvents only a locally excited (LE) emission from a moderately polar excited state is observed.[15,16] An additional, red-shifted emission is found in more polar solvents,[14] but even in cyclohexane a weak intramolecular charge-transfer (ICT) shoulder is found.[15] The origin of this red-shifted fluorescence is still not unquestioned. Various excited-state relaxation models have been proposed for interpretation of this dual-fluorescence phenomenon and both the twisted intramolecular charge-transfer (TICT) and planar intramolecular charge-transfer (PICT) models are the most extensively discussed explanations. Within the TICT model,[17−19] the untwisted dimethylamino (electron donor) unit rotates after photoexcitation toward an orthogonal orientation of the donor group relative to the aromatic ring system. In apolar solvents, DMABN emits only from the planar LE state, whereas a second minimum at a twisted conformation on the excited-state energy surface is populated in more polar environments. This twisted excited-state minimum corresponds to a ground-state maximum resulting in a smaller S_1-S_0 energy gap and red-shifted fluorescence as a consequence. Zachariasse and co-workers[15,20] explained the dual fluorescence by the so-called Pseudo-Jahn−Teller coupling. This model requires a sufficiently small energy gap between the first and second excited states, which allows an efficient vibronic coupling resulting in an increased mixing between both states. Later on,[21] this model was modified and the acronym PICT was introduced. Within the PICT[21] model, the pyramidal sp^3-amino nitrogen planarizes in its first excited state. More efficient conjugation results in a charge transfer from the donor to the acceptor group.

In the first two parts of this work we summarize experimental and theoretical results on DMABN. We then report the effect of both method and basis set on the optimized ground-state geometry of 4-aminobenzonitrile (ABN). This derivative of DMABN has been chosen because of the published accurate (cf. Section 3) experimental data regarding pyramidalization. The optimal basis set and method are then used for optimization

TABLE 1: Comparison of Calculated Geometries for ABN with Experimental Data[a]

method	basis set	δ	θ	ω	$d(C_1-N)$	energy
exp.[b]		0.0		34	1.37	
exp.[c]		0.0		42		
AM1		0.0	22.1	35.6	1.390	−215.7384[d]
HF	STO-3G	0.0	31.2	51.5	1.436	−372.7676
	3-21G	0.0	0.0	0.0	1.365	−375.3666
	6-31G*	0.0	23.7	38.1	1.382	−377.4699
	6-31G**	0.0	22.2	35.9	1.379	−377.4777
	6-31+G**	0.0	22.0	35.2	1.380	−377.4888
MP2	6-31G*	0.0	27.8	43.3	1.396	−378.6669
	6-31G**	0.0	27.9	43.4	1.396	−378.6861
	6-31+G**	0.0	27.3	41.5	1.398	−378.7103
DFT	VDZP	0.0	16.3	25.4	1.374	−379.5778
	TZV	0.0	0.0	0.0	1.38	−379.8669
	TZVP	0.0	20.6	32.5	1.383	−379.9779

[a] For definition of the twist angle δ (in degrees), wagging angle θ (in degrees), inversion angle ω (in degrees), and bond distance $d(C_1-N)$ (in angstroms), see Figure 1. Energy in Hartree. For HF and MP2, hydrogen polarization functions only on amino group. [b] Ref 41. [c] Ref 40. [d] Electronic energy; corresponds to $\Delta H = 50.80$ kcal/mol.

of DMABN. In the second part, the excited-state geometries are optimized by using both semiempirical Austin model 1 (AM1)/CISD and ab initio HF/CIS methods; the resulting structures are compared and analyzed. In the third part, the absorption energies are calculated with the ground-state optimized geometry using both semiempirical, ab initio and DFT-based methods, and the results are discussed with respect to experimental data. Further, the properties of the TICT state are calculated with the same methods. Finally, the excited-state reaction energetics are discussed comparing the different methods for (*i*) the planar LE and TICT state, (*ii*) twist-angle dependence of both the LE, and (*iii*) the L_a/CT state, respectively, for planar and twisted geometries. The results allow a conclusion regarding which optimization method yields the more correct geometries and whether ground-state geometries are sufficient to describe the excited-state processes. Further, a statement is presented about the advantages and disadvantages of the different methods for calculation of excited-state properties with the example of DMABN.

2. Computational Methods

The ground-state geometry optimizations are performed with the AM1 Hamiltonian within the VAMP program package, version 7.0,[22] and for the HF and Møller−Plesset second-order perturbation theory (MP2) methodologies as well as at the DFT level with the B3LYP functional[23] with Gaussian98[24] with different basis sets as given in Table 1. The symmetry of the HF and MP2 geometric and electronic structures is restricted to the highest possible symmetry, which does not lead to imaginary frequencies. For AM1/CISD and DFT optimizations, no symmetry restrictions are considered. The geometries of the excited states of DMABN are optimized by the HF/CIS method[2] and a 6-31G(d) basis set[25] with polarization functions on heavy atoms[26] using Gaussian94[27] and by the AM1/CISD methods using VAMP7.0[22] with configuration interaction including all single and double excitations from the five highest occupied orbitals to the five lowest unoccupied orbitals (CISD = 10).

For DMABN, apart from the HF/CIS method (see above), the CASSCF method[4] is also used to calculate the potential energy and one-electron properties of DMABN at a given geometry for a given electronic state. To obtain consistent results over the whole potential-energy surface, the wave function is specified without symmetry restrictions, independently of the input geometry. The active space is designed to include all benzene and nitrile π and π^* orbitals as well as the amino nitrogen n orbital. In addition, the inclusion of one antibonding methyl orbital stabilizes the calculations significantly. Therefore, the active space comprises 12 active electrons distributed over 12 active orbitals. All 11 core orbitals are held frozen, and the remaining 22 valence orbitals are kept inactive. This orbital partitioning has already been used successfully in previous calculations.[28,29]

In addition, CASPT2 corrections[5,6] to the CASSCF reference are evaluated. All potential energies are obtained in the block-diagonal Fock-matrix approximation (CASPT2D), because no major differences to the iterative full solution of the system of linear equations for the first-order wave function (CASPT2F) have been found previously.[29] The values of the reference weight of the CASSCF wave function within the CASPT2 solution, which give information on the validity of the perturbational approach, are usually in the range of 0.5 to 0.7, depending on the underlying geometry and the specified state. This is about the limit of applicability of the CASPT2 method for systems of such size as estimated from the approximate formula given in ref 30. Points where it was not possible to prevent the reference weight from falling below these values are marked. Dipole moments and transition dipole moments are calculated from the CASSCF wave functions by means of the complete-active-space state interaction (CASSI) method.[31] The energy differences needed to obtain the corresponding oscillator strengths are evaluated from the CASPT2 calculations. The ANO-L[3s2p1d/2s] basis set[32] is used in the CASSCF and CASPT2 calculations, which is of similar quality as the basis set used in the geometry optimizations. The CASSCF and CASPT2 calculations are performed with the MOLCAS 4.1 program package.[33]

All DFT/CI calculations are performed with the TURBOMOLE[34,35] suite of programs. The B3LYP functional is used for all DFT/SCI calculations, and Becke's hybrid exchange-correlation functional (BHLYP)[36,37] is used for all DFT/MRCI calculations because it uses an optimized amount of the exact HF exchange integral.[10] An energy cutoff of 1.0 Hartree for the selection of the most important configurations yields CI results for the excitation energies, which converge to about 0.1 eV and is used for all calculations. The following basis sets are used: valence double[38] and triple[39] ζ Gaussian AO basis sets augmented with d-polarization functions at the carbon and nitrogen atoms (VDZP: C, N: [3s2p1d]; H: [2s] and VTZP: C, N: [5s3p1d]; H: [3s]).

The twist angle δ is defined as $\{\alpha(C_2-C_1-N-C') + \alpha(C_2-C_1-N-C'')\}/2$, the wagging angle θ as $\{\alpha(C_2-C_1-N-C') - \alpha(C_2-C_1-N-C'')\}/2$ and the inversion or pyramidalization angle ω according to Figure 1. For ABN, the angles are defined analogously with the methyl group substituted by hydrogen. Finally, all computations are performed without consideration of any environment: Gas-phase calculations are compared with experimental data obtained by conditions in vacuo, where possible. Where necessary, experimental data from apolar solvents are used for comparison, but this represents an approximation. We decided not to include solvent effects because environmental effects cannot be computed for all chosen methods.

3. Experimental Data

The analysis of the experimentally obtained structural parameters for ABN yields an untwisted ground-state geometry with a pyramidalization angle ω of 42° according to a

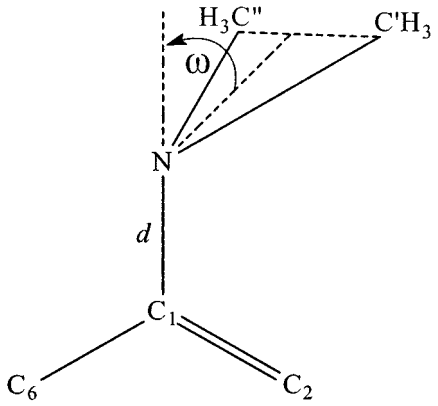

Figure 1. Enumeration of atoms, definition of the bond length *d*, and pyramidalization angle ω for DMABN.

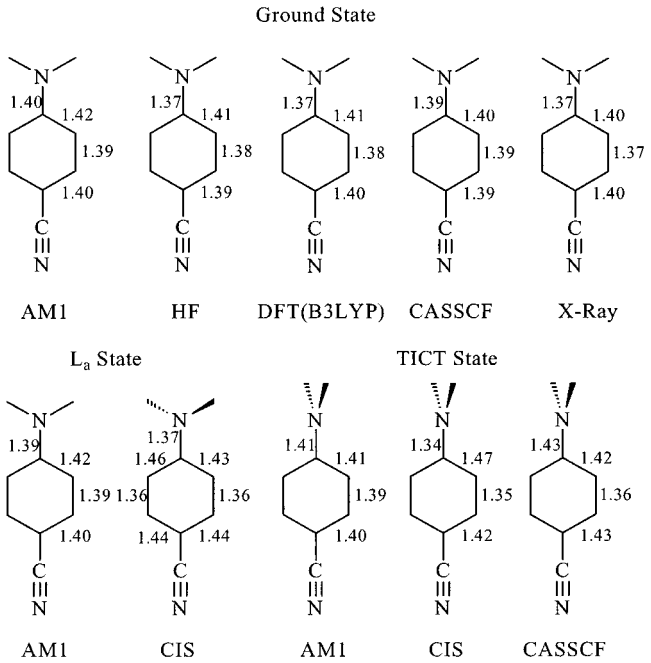

Figure 2. Optimized ground-state structure of DMABN: AM1 and HF/CIS (this work), DFT(B3LYP) (ref 77), CASSCF (ref 68), and X-ray structure (ref 41); optimized L_a state structure of DMABN: AM1 and HF/CIS (this work); optimized TICT state structure of DMABN: AM1 and HF/CIS (this work), and CASSCF (ref 68).

jet-experiment[40] and 34° according to an X-ray analysis.[41] Experimental data also show an untwisted but slightly pyramidal structure for the amino group of DMABN of 15° in the gas phase[42] and of 10.8°[41] and 7.1°,[43] respectively, in the crystal. The C_1–N bond is partly of double-bond character caused by the conjugation between the amino nitrogen and C_1 ($d_{exp} = 1.37$ Å),[41] and the aromatic unit consequently has alternating (quinoidal) bond lengths of 1.40 and 1.37 Å, respectively (see Figure 2). The ground-state rotation barrier for DMABN has been determined by Mackenzie and MacNicol to be 3000 cm^{-1} (7.55 kcal/mol).[44]

The first and second singlet excited states of DMABN are of L_b and L_a character, respectively. Excitation energies of 4.0 and 4.3 eV are reported from recent electron energy-loss experiments.[45] Absorption spectroscopy in an apolar solvent[15] determines somewhat higher energies of 35 600 cm^{-1} (4.4 eV) and 37 100 cm^{-1} (4.6 eV). The progression in the electronic excitation spectra under jet-cooled conditions suggests that the LE state is partly twisted by approximately 30°.[44,46] On the contrary, other fluorescence excitation experiments under isolated, supercooled conditions indicate that DMABN is planar in its LE state.[47] The development in energy of the first excited state as a function of the twist angle has been investigated experimentally by Wermuth[48] by the temperature dependence of the fluorescence quantum yield. He concludes that in alkane solvents, the TICT state is situated at an energy 8 kcal/mol higher than S_1 at planar geometry. In *n*-butyl chloride, the TICT state is already lower in energy than the primary excited L_b state by ca. 2 kcal/mol.[49,50] The endothermicity for the formation of the TICT state in the gas phase and in nonpolar solution is supported by Polimeno et al.[51] These authors extrapolated the experimental data and concluded that the TICT state is at 11.5 kcal/mol (0.50 eV) higher energy than the planar LE state. However, experimental data on the TICT state in the gas phase are available only for 2,6-*N*,*N*-tetramethylaminobenzonitrile (TMABN). TMABN is twisted by ca. 60° in the electronic ground state, 59.3° according to an X-ray[41] and 63.6° according to an analysis of the molar absorption coefficient ϵ in the following equation:[52]

$$\epsilon(\delta) = \epsilon(0) \cos^2 \delta \qquad (1)$$

An excitation energy of 32 900 cm^{-1} (4.1 eV) has been measured for TMABN in methylcyclohexane[53] and *n*-hexane[52] as solvents. Considering the $\cos^2$ relationship for the rotation barrier in the ground state, a barrier of 2600 cm^{-1} (0.3 eV) results for a twist angle of 60° relative to the planar ground state. Thus, the S_1 state energy at $\delta = 60°$ is situated at 35 500 cm^{-1}, at higher energy relative than at $\delta = 0°$ (for DMABN). The latter value is very similar to that extrapolated by Wermuth[48] for DMABN at $\delta = 90°$. Under jet-cooled conditions, only the normal fluorescence from the L_b state has been observed for DMABN.[40] The gas-phase fluorescence energy of 32 333 cm^{-1} (4.0 eV) is lowered to 3.6−3.9 eV in cyclohexane.[15,49] Here, a second, lower energy CT band is found at 3.2 eV.

The dipole moments have been determined by time-resolved microwave conductivity (TRMC) to 6.6 D for the ground state, 9.7 D for the LE state, and 17 D for the CT state in cyclohexane.[15] Even for alkane solvents, the experimental dipole moment will always be measured larger than in the gas phase because of the solute polarizability. Two recently published time-resolved resonance Raman studies[54,55] have established the transferred electron to be delocalized over the benzonitrile unit[54] and locate a downshift of 96 cm^{-1} for the phenyl-amino vibration in the CT state of DMABN, relative to the ground state.[55] The decisive C_1−N vibrational stretch band has been localized by comparison of the IR spectra of DMABN with those of a ^{15}N isotopically substituted derivative at the dimethylamino nitrogen. These results clearly account for a lengthening of the C_1−N bond, loosening of the phenyl ring, and lengthening of the cyano group in the CT state. Thus, the TICT model is favored to account for the properties of the CT state, and the PICT model is less well suited for explanation because it implies that the C_1−N bond has increased double-bond (quinoid) character with respect to the ground state. On the other hand, infrared studies by Okamoto et al.[56] and Okamoto[57] suggest that the quinoid character of the aromatic carbon atoms in DMABN in its CT state accounts for the PICT model because only this model is in accordance with the experimentally observed alternating bond lengths of the benzene unit in the CT state. However, the TICT model also may exhibit some quinoidal character in the aromatic system (cf. Chapter 4).

4. Comparison of Theoretical Calculations

Numerous theoretical investigations have been published for interpretation of the unusual fluorescence properties of DMABN.

Although the size of the molecule allows an investigation by qualitatively high first-principle methods, semiempirical methods are still applied (e.g., Purkayastha et al.[58] in 1999). However, several previously published papers using semiempirical Hamiltonians have yielded important results (e.g., see refs 59 and 60). The correct reproduction of the electronic ground-state geometry ($\delta = 0°$, $\omega = 10-15°$)[41,42] already represents a difficult task. Both semiempirical AM1[61] ($\delta = 0°$, $\omega = 18°$) and DFT calculations at the triple-ζ with two polarization functions (TZ2P) level[62] ($\delta = 0°$, $\omega = 14.2°$) are in good agreement with the experimental inversion angle of DMABN. An early HF/STO-3G[63] ground-state optimization significantly overestimates the inversion angle ($\omega = 38°$), whereas the HF method using a more sophisticated cc-pVDZ basis set[64] calculates an inversion angle ω of 15°. The semiempirical modified neglect of differential overlap (MNDO) parametrization predicts a ground-state minimum[65] with an twist angle of 50°, which is in clear contrast to both experiment and all other theoretical methodologies. The INDO/1 Hamiltonian does not reproduce the experimentally observed inversion angle ($\delta = 0°$, $\omega = 0°$).[59]

Excited-state optimized geometries are important for the investigation of emission properties because structural relaxation after photoexcitation cannot be reproduced by ground-state optimizations. Especially the calculation of TICT emission energies requires both ground- and excited-state optimized geometries. In the electronic ground state, the twisted ($\delta = 90°$) conformation represents a saddle point with a significantly pyramidalized nitrogen atom.[27,61,62] In contrast, the excited TICT state is characterized by a twisted and nonpyramidalized ($\delta = 90°$ and $\omega = 0°$) structure.[63,67] Use of the ground-state optimized geometry at $\delta = 90°$ for calculation of the TICT state can thus not reproduce the emission energy because the amino group of the optimized twisted ground-state geometry (i.e., at a fixed twist angle of 90°) increases its pyramidalization upon twisting.[63,61,66] Kato et al.[63] calculated [HF/CIS(STO-3G)] a saddle point at $\delta = 90°$ for the first excited state of DMABN with a wagging angle (which is not defined; see next section) of approximately 40°. Only ground-state-optimized geometries have been used. The semiempirical AM1 investigation by Gorse and Pesquer[67] as well as first-principle studies, e.g., using the CIS[29] and CASSCF[68] methods with optimized excited-state geometries, clearly represent an improvement for the quality of the results, although we do not clearly know the corresponding experimental structures.

The definition of the structural parameters represents a severe problem for comparison of theoretical results for DMABN with experimental data. Especially the terms *wagging angle* and *inversion angle* are used in the literature somewhat arbitrarily. Experimentally, the inversion angle is defined as the angle between the two planes spanned by the phenyl unit and the plane of the amino nitrogen with the two methyl carbon atoms, denoted as ω in this article. This angle, for example, is labeled wagging angle by Gorse et al.[67] The wagging angle θ is defined as $\{\alpha(C_2-C_1-N-C') - \alpha(C_2-C_1-N-C'')\}/2$ as used, for example, by Sudholt et al.[29] and Mennucci et al.[69] However, both angles describing the pyramidalization of the amino nitrogen are different and cannot be compared directly. For DMABN, the experimentally observed pyramidalization of 15°[41] corresponds to the theoretically obtained inversion angle ω and not to the wagging angle θ, which is about 10−20° smaller than ω. Kato and Amatatsu[63] did not give a definition of the wagging angle at all.

A controversy is found in the literature for the structure of the first excited state of DMABN, namely the LE (^1L_b) state. Geometry optimizations at the ab initio CIS level assign a partly twisted structure to the less polar first excited state of DMABN: $\delta = 22°$ by the HF/CIS(D95) study of Lommatzsch and Brutschy[64] and ca. 30° by the HF/CIS(6-31G**) study of Scholes and co-workers.[70] In refs 64 and 70, this partly twisted geometry is therefore assigned to the ^1L_b state. However, Sobolewski and co-workers[28] noted in their publication that the LE(L_b) was erroneously defined by Scholes et al.[70] because of interchanged L_a and L_b states at the CIS/6-31G* level of theory. In contrast, a planar structure of the LE state has been computed both by the CASSCF method as published by Chudoba et al.[71] and Roos[72] as well as by semiempirical studies.[67,66] The recent CASSCF excited-state optimization by Dreyer and Kummrow[68] yielded two LE states both of planar ($\delta = 0°$ and $\omega = 0°$) and pyramidal ($\delta = 0.0°$ and $\omega = 25.0°$) structure. However, only the planar conformation is in agreement with experimental infrared band intensities.[73]

Various articles have been published considering the evolution in energy of the first excited states as a function of either the twist angle δ or inversion angle ω. Most studies use only ground-state optimized geometries (e.g., see ref 72) or excited-state optimizations with symmetry restrictions (e.g., see refs 28 and 29). In several studies,[62,72,74] the TICT state is at significantly lower energy than the planar S_1 state. The formation of a TICT state in DMABN is hindered in this exothermic reaction only by the rotation barrier. The TDDFT study by Cammi et al.[74] calculates a decrease in energy from $\delta = 0°$ to $\delta = 90°$ by 11 kcal/mol. Only a few first-principle calculations of two-dimensional contour maps of excited state(s) potential energy surfaces studies have been published with both the pyramidalization and twist angle as parameters. Kato and Amatatsu[63] applied the HF/CIS method by using a CI with single, double, and triple excitations (CISDT) scheme with 10 active orbitals, which yielded an increase in the S_2 (CT) state energy by approximately 0.7 eV from the planar ($\delta = 0°$ and nonpyramidalized) minimum toward the TICT state minimum ($\delta = 90°$ and nonpyramidalized), which is more than 0.5 eV higher than the first excited state at $\delta = 90°$. In 1990, such calculations were only feasible by using the minimal STO-3G basis set. Although the calculated endothermic reaction is in agreement with the experimental study by Polimeno et al.,[51] we have some doubts about the reliability of the computed numbers. First, the minimal STO-3G basis set does not correctly reproduce the ground-state geometry and significantly overestimates the pyramidalization angle. Second, the nitrogen is generally assumed to be of sp^2 hybridization in the TICT state. On the contrary, the calculations by Kato et al. compute a pyramidalized sp^3-hybridized nitrogen atom. Thus, the agreement with experimental data is a result of the energy shift applied in ref 63.

The CASPT2 study by Serrano-Andrés et al.[72] also yields a twisted ($\delta = 90°$) and pyramidal ($\omega = 21°$) TICT state as the geometry of lowest energy on the first excited-state surface. In contrast to the experimental evidence[48] and the study by Polimeno et al.,[51] this TICT state is at lower energy than the planar S_1 state, i.e., the twisting coordinate is an exotherm reaction. Recently, Mennucci et al.[69] reported a similar two-dimensional energy surface based on multireference perturbated CIS calculations yielding the correct nonpyramidal ($\omega = 0°$) minimum at about $\delta = 80°$. This TICT state is by 0.1 eV (2.2 kcal/mol) higher in energy relative to the planar ($\delta = 0°$ and $\omega = 0°$) S_1 state minimum conformation. Also, a qualitatively high CASSCF[68] investigation with excited-state optimized geometries and an earlier ZINDO/S study[59] locate the TICT state at higher energy than the S_1 state minimum at planar conformation.

The detailed geometrical structure of the hypothetical TICT state is far from being experimentally and theoretically resolved. The symmetry-restricted HF/CIS excited-state optimization by Sobolewski and Domcke with a 3-21G basis set[75] yields an aniline unit with highly alternating bond lengths ($N-C_1$, 1.34 Å; C_1-C_2, 1.47 Å; C_2-C_3, 1.35 Å; C_3-C_4, 1.41 Å). The predicted short bond length $N-C_1$ of 1.34 Å is explained by strong Coulomb interactions between the positively charged amino group and the negatively charged benzonitrile unit (harpooning effect). Scholes and co-workers localized this TICT state as a transition state between two equivalent LE geometries with the same HF/CIS formalism but a qualitatively higher basis set (6-31G**). This clearly shows the difficulties of the HF/CIS method with this kind of problem. The recent CASSCF optimization of the DMABN TICT state by Dreyer et al.[68] also calculated alternating bond lengths within the benzene ring (C_1-C_2, 1.42 Å; C_2-C_3, 1.36 Å; C_3-C_4, 1.43 Å) but a significantly longer C_1-N bond length of 1.43 Å relative to the ground state (C_1-N, 1.39 Å). According to the authors, the twisting diminishes the shortening caused by conjugation effects of the C_1-N bond that is partly of double-bond character in the planar geometry. A shortened C_1-N bond in the TICT state was also found by an AM1/CISD study of Gedeck and Schneider[66] ($d(S_0) = 1.39$ Å, $d(S_{TICT}) = 1.33$ Å). Moreover, the degree of twisting of DMABN in the TICT state is ambiguous because several theoretical studies predict the energetic minimum of the TICT state at significantly smaller twist angles than $\delta = 90°$: A DFT/SCI[62] investigation calculates $\delta = 60°$ and partially allowed character for the "TICT state" by using ground-state optimized geometries. A shallow minimum at 45° has also been computed in two recently published studies by Sobolewski et al.[28] and Sudholt et al.[76] Here, the HF/CIS methodology is used for optimization of the first and second excited states and the energies are then determined by the CASPT2 method. The CASPT2 study by Serrano-Andrés[72] also localizes the TICT minimum at smaller twist angles ($\delta = 60°$ with ground-state geometries and the amino group forced to a sp^2 hybridization). An identical calculation with the inversion angle set to 21° reveals the TICT state at 90° at significantly lower energy than for $\omega = 0°$. Both a recent DFT/MRCI investigation[77] with ground-state optimized geometries and a study using CASSCF optimized excited-state geometries[68] predict the TICT state as completely decoupled and nonpyramidal ($\delta = 90°$ and $\omega = 0°$).

It becomes obvious that a lot of different excited-state geometries, potential surfaces, and reaction paths have been published not only using different methods and (symmetry) restrictions but also within one method with different basis sets. It is therefore important to emphasize that the main goal of this article is to investigate the photophysical properties of DMABN by a direct and better-defined comparison of various theoretical models with each other and with experimental data to elaborate the strengths and weaknesses of a given method.

5. Results and Discussion

5.1. Electronic Ground-State Geometry Optimization. *5.1.1. ABN Test for Basis Set and Methods.* Our first goal is to investigate the effect of both method and basis set on the geometry of ground-state-optimized DMABN. In particular, the slight pyramidalization of the dimethylamino group is a sensitive parameter for the quality of both the method and the basis set. In a series of benchmark calculations, the structure of the related molecule ABN is determined before DMABN and compared with the detailed experimental data available (see Table 1). The geometry of ABN is optimized in its electronic ground state by using semiempirical AM1, ab initio HF, MP2, and DFT/B3LYP methodologies and basis sets of different quality, varying from STO-3G to TZVP. A nontwisted geometry of ABN is found by all methods, whereas polarization functions are imperative to reproduce the experimentally observed amino group pyramidalization. Both HF/3-21G and DFT/B3LYP/TZV basis sets without polarization functions yield a planar C_{2v} geometry for ABN. The AM1 result of $\omega = 35.6°$ is in qualitatively good agreement with the experimental data of $\omega = 42°$ in a jet-cooled experiment[40] and of $\omega = 34°$ in an X-ray analysis.[41] HF/STO-3G strongly overestimates the pyramidalization ($\omega = 51.5°$) and also the carbon−amino nitrogen bond distance ($d_{HF} = 1.44$ Å; $d_{exp} = 1.37$ Å[41]) corroborates the well-known deficiencies of the minimal basis set. The MP2 results somewhat overrate the pyramidalization ($\omega \approx 42°-43°$) and the C_1-N distance ($d \approx 1.40$ Å) in comparison with the X-ray values, which may however be subject to packing effects and hydrogen bonds. The DFT methods slightly underestimate the pyramidalization ($\omega \approx 30°$) and correctly reproduce the C−N distance ($d = 1.37-1.38$ Å). In general, an increased C_1-N (see Figure 1) bond length is calculated for larger pyramidalization angles, reflecting the increased sp^3 character and decreased conjugation of the amino nitrogen with the aromatic benzene system. The results are in agreement with a recent study on aniline, where similar results were obtained.[78] Neither the further addition of diffuse functions (HF/6-31+G* resulting in $\omega = 35.2°$) nor additional polarization functions at the amino hydrogens (HF/6-31G** resulting in $\omega = 35.9°$) improve the results with respect to the experimentally observed structural data. One should, however, be aware that hydrogen atoms cannot be located precisely by X-ray spectroscopy.

5.1.2. DMABN. For optimization of DMABN in its electronic ground state, both methods are applied that will be used for optimization of the excited states, namely the AM1 and HF methodologies. The results are summarized in Table 2 and Figure 2. Both methods reproduce the experimentally observed pyramidalization. The semiempirical AM1 Hamiltonian calculates a pyramidalization angle of 24.7° and also the HF optimization yields a pyramidal amino nitrogen of 14.8° ($\omega_{exp} = 15°$).[41] The larger angle ω of the AM1 Hamiltonian results in a calculated C_1-N bond distance of 1.40 Å, which is too long as compared with the experimental data ($d_{exp} = 1.37$ Å[41]). The angle ω as obtained by the HF method is in perfect agreement with experimental data, and also the bond length of $d = 1.37$ Å fits excellently to the X-ray data. The results of

TABLE 2: Comparison of Calculated Optimized Geometries for DMABN in Ground and Various Singlet Excited States with Experimental Data[a]

method	name[b]	state	δ	θ	ω	$d(C_1-N)$	methyl position[c]
AM1	GS	S_0	0.0	15.8	24.7	1.399	syn1
AM1/CISD	LE	L_b	0.0	0.7	1.1	1.389	syn1
	(P)ICT	L_a	0.0	0.5	0.7	1.389	syn1
	TLE	L_b	89.9	24.9	45.0	1.437	syn2
	TICT	L_a	90.0	0.0	0.0	1.412	syn1
HF	GS	S_0	0.0	8.8	14.8	1.374	syn1
HF/CIS	ICT	L_a	34.8	12.4	19.7	1.367	syn2
	TLE	L_b	90.0	25.0	44.2	1.414	syn2
	TICT	L_a	90.0	0.0	0.0	1.341	syn1
exp.	X-ray[d]	S_0	0.0		10.8	1.365	
	Vacuum[e]	S_0	0.0		15		

[a] GS = Ground State, LE = Locally Excited State, (P)ICT = (Planar) Intramolecular Charge Transfer State, TLE = Twisted Locally Excited State, TICT = Twisted Intramolecular Charge Transfer State. [b] See Figure 2 for explanation. [c] Ref 41. [d] Ref 42.

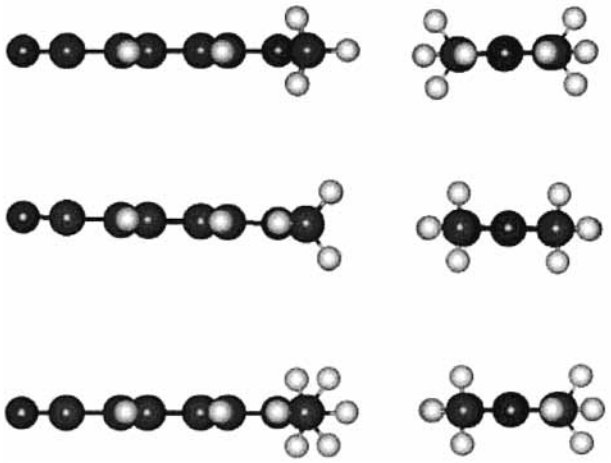

Figure 3. Side (left) and front (right) view of DMABN with *syn1* (top), *syn2* (middle), and *anti* (bottom)-methyl group orientation.

optimizations with different configurations of the methyl groups illustrate that the relative orientation of the two methyl groups also has to be considered when analyzing the structure of DMABN.

In principle, three different minimum-energy orientations are possible as shown in Figure 3. In the *syn1* conformation, one hydrogen atom of each methyl group faces the other one and both are in the plane of the phenyl unit (d(H−H) = 2.12 Å). In the *syn2* conformation two hydrogen atoms of both methyl groups oppose each other, whereas for the *anti* conformation the methyl groups are staggered. The orientation of the methyl group has an important influence on the geometry of the optimized ground state. *Syn1* represents the global minimum conformation with $\delta = 0.0°$ and $\omega = 24.7°$. For the *syn2* conformation, a local AM1 minimum with a twist angle of 30° and inversion angle ω of 33° is calculated at 0.70 kcal/mol higher energy. The *anti* or *eclipsed* conformation also represents a local minimum at 0.5 kcal/mol higher energy relative to the *syn1* minimum. The smaller distance between the two closest hydrogen atoms in the *anti* conformation of 1.88 Å disfavors this orientation relative to the untwisted *syn1* conformation.

5.2. Electronic Excited-State Geometry Optimization. In this section we investigate the differences and analogies of two methods routinely available for optimization of excited states of larger molecules with more than 10 non-hydrogen atoms, AM1/CISD and HF/CIS. Four geometries are optimized and the results are summarized in Table 2 and Figure 2. The L_b and L_a states of DMABN correspond to S_1 and S_2 optimized by using the ground-state-optimized conformation as starting geometries. Because the L_a and L_b states lie energetically very close together in the HF/CIS method and root flipping easily leads to a collapse of the higher excited state during energy minimization, it is only possible to optimize the lowest excited state in each symmetry. Therefore, the electronic state and the steric conformation of DMABN are specified by symmetry restrictions for the optimization with this method. The S_1-optimized geometry is generated by an overall optimization of the first excited singlet state within C_1 symmetry. The resulting slightly twisted and pyramidalized S_1 state has mostly L_a character, because this state is usually lower in energy than the L_b state within the HF/CIS method.[28,29,70,79] The structure is therefore named ICT throughout the article.

Two local minima exist at the fully twisted geometry of the dimethylamino group (i.e., δ fixed to 90°): The "twisted locally excited state" (TLE) corresponds in electronic character to the planar L_b state and is strongly pyramidalized ($\theta = 25°$ in both

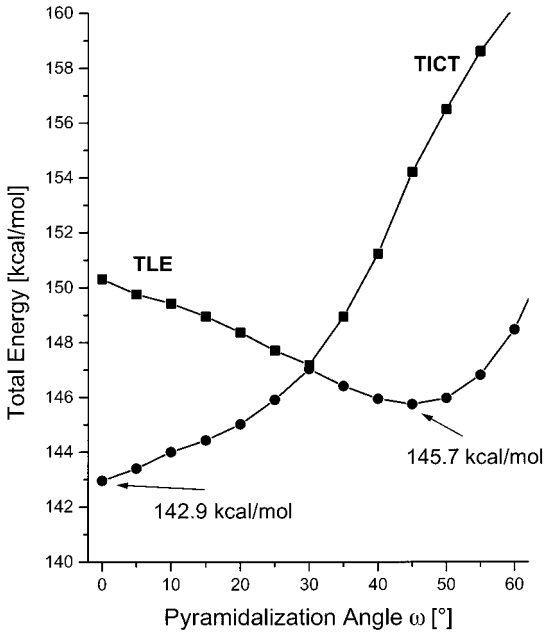

Figure 4. Energies for locally excited (TLE) and TICT state of twisted DMABN ($\delta = 90°$) as a function of the inversion or pyramidalization angle ω.

HF/CIS and AM1/CISD methods; see Table 2). In contrast, the optimized TICT state is nonpyramidal and of C_{2v} symmetry. This state is related to the L_a state at planar conformation. The TICT state is not the global L_a-like completely twisted minimum within the HF/CIS calculations. A second L_a state with *syn2* methyl groups is located at lower energy than the TICT state of L_a character (C_{2v} symmetry, $\delta = 90°$, and $\omega = 0°$). Further relaxation of the lowest L_a state within C_2 symmetry results in a TICT state with the methyl groups oriented in an *anti* position. This geometry may be adiabatically connected to the transition structure found by Scholes et al.[70,79]

The results as summarized in Table 2 reveal the following properties: AM1/CISD calculates the less polar L_b state [μ = 6.9 D, mainly highest occupied molecular orbital (HOMO)→lowest unoccupied molecular orbital (LUMO)+1 character, ΔH_f^0 = 124.9 kcal/mol] at lower energies than the more polar L_a state (μ = 10.2 D, mainly HOMO→LUMO character, ΔH_f^0 = 135.9 kcal/mol) in agreement with experimental data. Both states differ only negligibly in their geometry. The structures reveal an untwisted ($\delta = 0°$) and insignificantly pyramidal amino group ($\omega = 0.7°$ and $\omega = 0.5°$, respectively) with *syn1* orientation of the methyl groups. A second local minimum with *anti* orientation of the methyl groups is calculated 3.39 kcal/mol higher in energy (ΔH_f^0 = 139.4 kcal/mol) with a partly twisted and pyramidal geometry ($\delta = 29°$ and $\omega = 25°$). For the twisted orientation of the dimethylamino group ($\delta = 90°$), the character of the first excited state depends on the amount of inversion (see Figure 4). The highly polar TICT state with *syn1* conformation (μ = 14.3 D, mainly of HOMO→LUMO character) calculated with AM1/CISD has the lowest energy at δ = 90° (ΔH_f^0 = 142.9 kcal/mol). The inversion angle is zero, and the total energy of the TICT state increases significantly when pyramidalizing the amino group. In contrast, the twisted weakly polar L_b state (TLE state, HOMO−2→LUMO and HOMO−1→LUMO+1 excitation) has a higher lying minimum in energy (ΔH_f^0 = 145.7 kcal/mol) and a small dipole moment (μ = 3.5 D) at $\omega = 25°$ and *syn2* conformation. The sp^2-hybridized TICT state is 2.8 kcal/mol lower in energy than the TLE state. Figure 4 shows the evolution in energy of both twisted states as a

function of the inversion angle. The picture clearly shows that both the TICT and the TLE state represent two local minima on the excited-state surface (for δ fixed to 90°) characterized by different inversion angles. The energy profiles are quite similar to those calculated by CASPT2 on HF/CIS geometries.[29] The C_1-N bond length of 1.41 Å and the small differences in the bond lengths of the phenyl unit (see Figure 2) clearly account for two decoupled units. In the TICT state, the negatively charged aromatic benzonitrile acceptor unit is separated from the positively charged dimethylamino donor group by a bond of single-bond character. The missing conjugation is counterbalanced by the attracting interactions between the donor and acceptor units, which are differently weighted ($d = 1.41$ Å in AM1/CISD and $d = 1.34$ Å in HF/CIS, as compared with $d = 1.43$ Å in CASSCF [68]). We also point out the inconsistent AM1/CISD results for the C_1-N bond length obtained in this work ($d = 1.41$ Å) and by Gedeck and Schneider[66] ($d = 1.33$ Å).

HF/CIS calculates the L_a state for small twisting and inversion angles at lower energies than the L_b state in contrast to experimental data.[14] The experimentally observed state order can be reproduced correctly only with a sufficiently large basis set like 6-311++G(2d,p) as used in the work of Scholes et al.[79] However, we decided not to use this large basis set because it is uneconomical to combine a high-quality basis set with a method including only single excitations. Thus, only the L_a-optimized geometry is presented in Table 2. This partly twisted optimized geometry ($\delta = 34.8°$ and $\omega = 12.4°$) has a *syn2* orientation of the methyl groups. This geometry is comparable with the HF/CIS optimized geometry with a twist angle of approximately 30° and *syn2* orientation as published by Scholes et al.[70] and attributed to the L_b state as well as by Sobolewski et al.[28] and attributed to the L_a state. The clear distinction between *syn1* and *syn2* conformations becomes challenging for a large pyramidalization angle. Thus, the HF/CIS *syn2* geometry of the L_b state is obtained by starting with the planar *syn1* ground-state conformation and increasing the pyramidalization. The AM1/CISD calculations show that both geometries represent a local minimum on the excited-state hypersurface with the nearly planar form as the global minimum. Only the HF/CIS optimization yields the somewhat twisted *syn2* geometry as the global minimum. We decided to perform all forthcoming excited-state calculations by using both geometries. It thus becomes possible to determine the geometry of the L_b state by a direct comparison of calculated and experimental absorption energies by using both computed conformations.

The HF/CIS and AM1/CISD structures for the TICT state differ significantly in the bond length between the amino nitrogen and the adjacent carbon atom C_1 (see Table 2 and Figure 2). This bond is significantly shorter in the HF/CIS optimized geometry [$d(C_1-N) = 1.341$ Å] and the uncoupled benzene subunit possesses alternating bond lengths. In general, rotation of the dimethylamino group increases the carbon−nitrogen bond length because of decreasing conjugation. Both AM1/CISD ($\Delta d = +0.037$ Å) and HF/CIS ($\Delta d = +0.028$ Å) calculate a larger C_1-N distance for the TLE state as compared with the ground state where charge transfer is insignificant in both cases. Planarizing the pyramidal amino group increases the donor strength[80] and lowers the highly polar TICT state below the TLE state. The induced significant CT character leads to a shortened bond length because of attracting Coulomb interactions of the positively polarized dimethylamino donor group and the negatively polarized benzonitrile acceptor subunit. However, AM1/CISD yields only a slight shortening of the C_1-N bond length by $\Delta d = -0.025$ Å, whereas HF/CIS calculates $\Delta d = -0.073$ Å compared with the TLE state at the TICT state geometry. A longer C_1-N bond length results for AM1/CISD but a shorter for HF/CIS relative to the nontwisted optimized ground state. CASSCF optimizations by Dreyer et al.[68] also obtain a bond widening from 1.386 Å for the ground state to 1.434 Å for the sp^2-hybridized TICT state, but the structure of the benzonitrile unit is quinoid in this case (Figure 2). The CASSCF and AM1/CISD methods both predict a predominating effect of the missing conjugation (i.e., increased C_1-N bond length); the CASSCF and HF/CIS methods both predict a quinoid benzonitrile geometry. Summarizing, the three methods compute three different geometries for the TICT state and no final conclusion about the reliability of each method is possible, because no experimental data on the relaxed geometry of the TICT state are available.

5.3. Absorption Energies. In Table 3, which is based on the AM1- and HF-optimized ground-state geometries, the single-point excitation energy calculations are compared for the excited-state properties by using the following methods: The semiempirical AM1/CISD, ab initio HF/CIS, CASSCF, and CASPT2, as well as the DFT-based TDDFT, DFT/SCI, and DFT/MRCI methods. For all methods (except AM1), a valence double-ζ basis set including polarization functions has been used. In addition, the basis set effect has been investigated by comparing DFT/MRCI(B3LYP)/VDZP with DFT/MRCI-(B3LYP)/TZVP results.

A direct comparison of the data in Table 3 reveals the expected similarity of excited-state properties for both ground-state geometries. The excitation energies for the AM1 ground-state-optimized geometry are generally lower by less than 0.1 eV, but the dipole moments, oscillator strengths, and characterization of both the L_b and L_a states are comparable for both geometries. Because the AM1 geometry shows a larger pyramidalization angle ω, this can be connected to the slightly lowered absorption energies. The L_b state is a combination of the HOMO→LUMO+1 and to a lesser degree of the HOMO−1→LUMO excitation. The L_a state is mainly of HOMO→LUMO character for all methods. According to the results of Table 3, both the AM1/CISD and HF/CIS methods cannot be used for reproduction of experimental absorption energies. AM1/CISD underestimates the excitation energies by ca. 0.5 eV and the dipole moments are too small [$\mu(L_a)_{AM1/CISD} = 9.7$ D vs $\mu(L_a)_{exp} = 11-14$ D[17]]. On the other hand, HF/CIS overestimates the excitation energy by 1.0−1.5 eV and locates the L_a state with an even smaller dipole moment of 8.4 D at lower energies than the L_b state. Energy correction by CASSCF reproduces the correct ordering of the states, but both the L_b and L_a state energies are calculated too high by ca. 0.5 eV (L_b) and 1.5 eV (L_a) relative to the experimental data. The CASSCF dipole moments with $\mu = 6.1-6.7$ D for L_b and $\mu = 12.8$ D for L_a are at the lower border of the values measured in nonpolar solvents, which should be higher than in the gas phase because of polarization effects. Further energy correction by perturbation theory (CASPT2) brings the energies down close to the experimental absorption energies ($L_b = 4.1$ eV; $L_a = 4.4$ eV). TDDFT energies are calculated in the correct range, but as for CASPT2 excited-state dipole moments, could not be calculated here. Both DFT/SCI and DFT/MRCI reproduce experimental energies satisfactorily. The DFT/SCI dipole moments are calculated too high [$\mu(L_a)_{DFT/SCI} = 15.7$ D] but DFT/MRCI dipole moments are within the experimental range [$\mu(L_a)_{DFT/MRCI(VDZP)} = 12.6$ D]. Improvement of the basis set from VDZP to TZVP changes the results only slightly. The DFT/MRCI(B3LYP)/TZVP energies of 4.31 eV [$\Delta E_{exp} = 4.0$

TABLE 3: Total Energy (in Hartree), Excitation Energy ΔE (in Electronvolts), Dipole Moment μ (in Debyes), and Oscillator Strength f for the AM1- and HF-Optimized Ground-State Geometry of DMABN[a]

		AM1				HF			
method	state	energy[b]	ΔE	μ	f	energy[b]	ΔE	μ	f
exp in jet[c]		0-0 band	4.0			0-0 band	4.0		
EEL exp.[d]	L_b		4.0				4.0		
	L_a		4.4				4.4		
exp in alkane[e]	L_b	0-0 band	3.6−3.9	6−10	0.04	0-0 band	3.6−3.9	6−10	0.04
	L_a	max.	4.4	15[f]	0.33[g]	max.	4.4	15[f]	0.33[g]
AM1/CISD	S_0	45.7		5.3		55.6		5.5	
	L_b	127.8	3.6	6.6	0.01	140.1	3.7	7.4	0.01
	L_a	137.6	4.0	9.7	0.34	147.7	4.0	9.5	0.32
HF/CIS(6-31G*)	S_0	−455.5077		7.0		−455.5201		7.3	
	L_b	−455.2933	5.8	7.8	0.02	−455.3037	5.9	8.3	0.03
	L_a	−455.2993	5.7	8.4	0.46	−455.3059	5.8	8.9	0.47
CASSCF(VDZP)	S_0	−455.7504		6.1		−455.7545		6.5	
	L_b	−455.5795	4.7	6.1	0.00	−455.5801	4.7	6.7	0.01
	L_a	−455.5297	6.0	12.8	0.47	−455.5313	6.1	12.8	0.48
CASPT2(VDZP)	S_0	−457.0401				−457.0336			
	L_b	−456.8890	4.1			−456.8802	4.2		
	L_a	−456.8799	4.4			−456.8681	4.5		
TDDFT(VDZP)	S_0	−458.1275		7.0		−458.1267		7.3	
	L_b	−457.9620	4.5		0.03	−457.9592	4.6		0.03
	L_a	−457.9552	4.7		0.50	−457.9483	4.8		0.51
DFT/SCI(VDZP)	S_0	−457.8401		7.0		−457.8591		7.3	
	L_b	−457.6872	4.2	10.8	0.02	−457.684	4.2	11.2	0.03
	L_a	−457.6713	4.6	15.7	0.63	−457.6664	4.8	15.4	0.65
DFT/MRCI(VDZP)	S_0	−457.8572		6.8		−457.8596		7.2	
	L_b	−457.6964	4.4	8.0	0.02	−457.6950	4.5	8.6	0.03
	L_a	−457.6955	4.7	12.6	0.63	−457.6823	4.8	12.7	0.64
DFT/MRCI(TZVP)	S_0	−458.3317		7.1		−458.3405		7.5	
	L_b	−458.1734	4.3	8.3	0.02	−458.1792	4.4	9.0	0.02
	L_a	−458.1635	4.6	12.8	0.63	−458.1666	4.7	13.0	0.63

[a] Experimental data from refs 14, 15, 49, 52, 81, and 82. [b] For AM1 in kilocalories per mole. [c] Ref 40. [d] Electron energy loss experiments, ref 45. [e] Refs 14, 15, 49, and 52. [f] Ref 81. [g] Ref 82.

TABLE 4: Total Energy (in Hartree), Excitation Energy ΔE (in Electronvolts), and Dipole Moment μ (in Debyes) for the AM1/CISD- and HF/CIS-Optimized TICT State Geometries of DMABN

	AM1/CISD			HF/CIS		
method	total energy[a]	ΔE	μ	total energy[a]	ΔE	μ
exp. in cyclohexane[b]		3.2	17		3.2	17
AM1/CISD	142.9	3.8	14.3	147.9	3.6	13.3
HF/CIS(6-31G*)	−455.2698	6.1	14.3	−455.2906	5.4	13.7
CASSCF(VDZP)	−455.5404	5.3	15.8	−455.5460	4.8	14.9
CASPT2(VDZP)	−456.8916	3.6		−456.8883	3.1	
TDDFT(VDZP)	−457.9957	3.1		−457.9957	2.8	
DFT/SCI(VDZP)	−457.6926	3.5	19.1	−457.6892	3.2	17.7
DFT/MRCI(VDZP)	−457.7023	3.8	16.6	−457.7015	3.5	15.3
DFT/MRCI(TZVP)	−458.1785	3.7	16.7	−458.1822	3.4	15.4

[a] For AM1 in kilocalories per mole. [b] Ref. 15.

eV,[40] 4.3 eV[45]] and 4.6 eV [ΔE_{exp} = 4.6 eV[45]] as well as dipole moments of 8.3 D (μ_{exp} = 8−11 D[15,17]) and 12.8 D (μ_{exp} = 11−14 D[15,17]) are in good agreement with experimental data as are CASPT2 energies and CASSCF dipole moments (taken the solvent influence on the measured values into account).

5.4. The TICT State. The optimized TICT geometries differ significantly for the benzene structure and the N−C_1 bond distance as reported in Section 4.2. We therefore also expect different TICT state properties for the HF/CIS-optimized structure with a short C−N bond length and a quinoid benzene structure and the AM1-optimized structure with a long C−N bond length and an aromatic structure of the benzene moiety.

The results as summarized in Table 4 (based on the AM1/CISD- and HF/CIS-optimized TICT state geometries) and Figure 2 corroborate this expectation. The geometry of the CASSCF optimization[68] yields a structure combining the characteristics of both the AM1/CISD and HF/CIS method. The carbon−amino nitrogen bond is of single-bond character (d = 1.43 Å), whereas the carbon atoms in the phenyl moiety show alternating single- and double-bond character (see Figure 2). Experimentally, a weak CT emission at 3.1−3.2 eV is observed in cyclohexane [15,48] with the main LE fluorescence band at 3.6−3.7 eV.[15,48] The large dipole moment, the forbidden character (f = 0), and the main HOMO→LUMO character of the TICT state is reproduced for all methods and for both optimized geometries (details not shown). Analysis of the molecular orbitals characterizing the TICT state describes this state as corresponding to a charge transfer from the amino nitrogen lone electron pair to a π^* orbital on the benzonitrile acceptor unit for all methods. In general, the energy of the TICT state calculated with the HF/CIS geometry is ca. 0.3 eV lower in energy relative to the AM1/CISD-optimized geometry. Both energies of 3.8 eV (AM1/CISD for AM1/CISD geometry) and 3.6 eV (AM1/CISD for HF/CIS geometry) agree fairly well with the experimental energy difference of 3.2 eV in alkane solvents.

Both the CASSCF (L_b/TLE = 4.7 eV; L_a/TICT = 4.8 eV) and the HF/CIS (L_b/TLE = 6.0 eV; L_a/TICT = 5.4 eV) energies at HF/CIS geometry are far too high compared with the experimental emission energy. The CASSCF dipole moments, however, are close to the measured values taking their solvent dependence discussed in Section 5.3 into consideration. CASPT2 correction results in a TICT state energy difference of 3.1 eV (HF/CIS geometry) and 3.6 eV (AM1/CISD geometry) in good agreement with experimental data of 3.2 eV.[15] For TDDFT, a TICT state energy difference of 3.1 eV is calculated by using the AM1 geometry, which is too low compared with the experimental data. For the HF/CIS geometry, an energy difference of 2.8 eV is calculated for the TICT state, which is even lower in energy. The DFT/SCI TICT energy gap is in good

TABLE 5: Total Energy (in Hartree), Excitation Energy ΔE (in Electronvolts), and Dipole Moment μ (in Debyes) for the AM1/CISD- and HF/CIS-Optimized L_a State of DMABN

	AM1/CISD			HF/CIS		
method	total energy[a]	ΔE	μ	total energy[a]	ΔE	μ
AM1/CISD	135.9	4.0	10.2	142.5	3.8	9.8
HF/CIS(6-31G*)	−455.3004	5.6	8.9	−455.3159	5.2	8.6
CASSCF(VDZP)	−455.5324	5.9	13.2	−455.5410	5.6	12.8
CASPT2(VDZP)	−456.8806	4.3		−456.8845	3.9	
TDDFT(VDZP)	−457.9568	4.7		−457.9537	4.5	
DFT/SCI(VDZP)	−457.6724	4.6	15.8	−457.6744	4.3	13.5
DFT/MRCI(VDZP)	−457.6880	4.6	12.9	−457.6894	4.4	9.9
DFT/MRCI(TZVP)	−458.1651	4.5	13.2	−458.1718	4.3	10.0

[a] For AM1 in kilocalories per mole.

TABLE 6: Total Energy (in Hartree), Excitation Energy ΔE (in Electronvolts), and Dipole Moment μ (in Debyes) for the AM1/CISD-Optimized L_b State of DMABN

method	total energy[a]	ΔE	μ
AM1/CISD	124.9	3.5	6.9
HF/CIS(6-31G*)	−455.2948	5.8	8.3
CASSCF(VDZP)	−455.5783	4.6	6.6
CASPT2(VDZP)	−456.8902	4.1	
TDDFT(VDZP)	−457.9624	4.5	
DFT/SCI(VDZP)	−457.6898	4.1	11.2
DFT/MRCI(VDZP)	−457.6991	4.3	8.5
DFT/MRCI(TZVP)	−458.1761	4.3	8.9

[a] For AM1 in kilocalories per mole.

agreement with experiment (AM1/CISD, 3.5 eV; HF/CIS, 3.2 eV) but the calculated dipole moment is too high (AM1/CISD, 19.1 D; HF/CIS, 17.7 D). The DFT/MRCI dipole moments are in much better agreement with experimental data (AM1/CISD, 16.6 D; HF/CIS, 15.3 D), and the TICT state energy difference (AM1/CISD, 3.8 eV; HF/CIS, 3.5 eV) is also more reliable. Improvement of the basis set further lowers the TICT state energy (AM1/CISD, 3.7 eV; HF/CIS, 3.4 eV). The experimentally red-shifted emission energy at 3.2 eV[15] deviates only by 0.2 eV from the DFT/MRCI(B3LYP)/TZVP TICT state energy by using the HF/CIS geometry. A recent DFT/MRCI(TZVP) study only using ground-state-optimized geometries[77] obtains 4.0 eV in comparison with 3.7 eV (AM1/CISD TICT state geometry) and 3.4 eV (HF/CIS TICT state geometry) for the gas-phase emission energy from the TICT state. This clearly shows the necessity of excited-state optimizations.

5.5. L_b and L_a Reaction Coordinate. The energies for the AM1/CISD- and HF/CIS-optimized L_a state of DMABN are summarized in Table 5, the AM1/CISD-optimized L_b state of DMABN in Table 6. No experimental data are available for energy differences between the planar and the twisted L_b (TLE) state. However, it is generally assumed that the LE state increases in energy along the twisting coordinate and that the formation of the twisted LE state is an endothermic process.[72] The results of all methods except those of CASSCF (ΔE = −8.08 kcal/mol; see Table 7) corroborate this hypothesis. The increase in energy varies significantly with the choice of the method from +7.7kcal/mol for TDDFT to +20.8 kcal/mol for AM1/CISD. The results of the most reliable CASPT2 (ΔE = 10.7 kcal/mol) and DFT/MRCI(BHLYP)/TZVP (ΔE = 12.4 kcal/mol) methods are both in the region of 11−12 kcal/mol, and we assume this increase in the LE state energy is a reliable estimate.

Similarly, no experimental data are available for the evolution in energy along the twisting coordinate for the polar L_a/CT state. We thus also compare our data with those of earlier calculations.

TABLE 7: Reaction Energetics for DMABN along the Twisting Coordinate in Kilocalories per Mole for Different Excited-State Geometries

	$L_b \rightarrow$ TICT[a]	$L_b \rightarrow$ TLE[b]	$L_a \rightarrow$ TICT[c]	
geometries	AM1/CISD[d]	AM1/CISD[d]	AM1/CISD	HF/CIS
AM1/CISD	18.0	20.8	7.0	8.4
HF/CIS	15.7	6.7	19.2	15.9
CASSCF	23.8	−8.1	−5.0	−3.1
CASPT2	−0.9	10.7	−6.9	−2.4
TDDFT	−20.9[e]	7.7	−24.4	−20.7[f]
DFT/SCI	−1.7	19.8	−12.7	−9.3
DFT/MRCI(VDZP)	−2.0	12.7	−9.0	−4.4[f]
DFT/MRCI(TZVP)	−1.5	12.4	−8.4	−3.0[f]

[a] $\Delta E(S_1)$ 90°−0°, i.e., $E(TICT) - E(LE)_{planar}$. [b] $\Delta E(L_b)$ 90°−0°, i.e., $E(TLE) - E(LE)_{planar}$. [c] $\Delta E(L_a)$ 90°−0°, i.e., $E(TICT) - E(La)_{planar}$. [d] The corresponding value for the HF/CIS-optimized geometry cannot be determined without symmetry restrictions. [e] S_2, S_1 is transition HOMO−LUMO. [f] S_1 mainly of HOMO−LUMO and minor HOMO−LUMO+1 character; S_2 vice versa.

Comparison of the calculations for both the HF/CIS and AM1 geometries reveals the differences whether a quinoid (HF/CIS) or aromatic (AM1/CISD) benzene group is a more reliable description of the TICT state, and whether a planar (AM1/CISD) or partly twisted and pyramidal (HF/CIS) structure describes best the LE state. In both cases, only the AM1/CISD and HF/CIS methods predict an increase of the L_a/ICT state energy along the rotation coordinate. The AM1/CISD TICT energy is higher in energy by 6.98 kcal/mol (AM1/CISD geometry) and 8.4 kcal/mol (HF/CIS geometry), respectively, than the planar L_a state. Gedeck and Schneider[66] found an increase in energy by approximately 10 kcal/mol in their AM1 study, Gorse and Pesquer[67] by ca. 7 kcal/mol, and the ZINDO/S study of Broo and Zerner[59] by ca. 2−3 kcal/mol. Comparing the results here (Table 7), the TICT state is higher in energy than the planar L_a state by 19.2 kcal/mol (AM1/CISD geometry) and 15.9 kcal/mol (HF/CIS geometry) with use of the HF/CIS methodology. Sobolewski and co-workers[28] calculated an increase in energy by ca. 12 kcal/mol. All other methods located the TICT state at lower energy than the optimized L_a state (Table 7). The exothermicity is generally lowered for the HF/CIS geometries by ca. 3−5 kcal/mol relative to the AM1 geometry. Also, the energy differences using the CASPT2 ($\Delta E_{AM1/CISD}$ = −6.9 kcal/mol; $\Delta E_{HF/CIS}$ = −2.4 kcal/mol) and DFT/MRCI(TZVP) ($\Delta E_{AM1/CISD}$ = −8.4 kcal/mol; $\Delta E_{HF/CIS}$ = −3.0kcal/mol) methods are of comparable size for each optimization method. The results are in qualitatively good agreement with the CASPT2 energy gain of ca. 7 kcal/mol as computed by Sobolewski et al.[28] with CIS-optimized geometries and of ca. 8 kcal/mol as determined by Dreyer et al.[68] with CASSCF-optimized excited state geometries. Again, the TDDFT method significantly overestimates the energy lowering of the TICT state by more than 20 kcal/mol, as also has been found by Cammi et al.[74] ($\Delta E \approx$ 23 kcal/mol).

5.6. Energetics on the S_1 Hypersurface [LE (L_b) to TICT Photochemical Reaction]. The energy difference between the primary excited L_b-optimized state (S_1) at planar geometries and the energy of S_1 at the TICT geometry determines whether the formation of the TICT state is an exotherm or endotherm process. The results using the AM1/CISD geometry are summarized in the first column of Table 7. No data are available for the HF/CIS geometries (see also Section 2) but the discussion in Section 5.5 shows that the energies using the HF/CIS geometries generally are about 3−5 kcal/mol higher than those using the AM1/CISD geometries. AM1/CISD (ΔE = 18.0 kcal/

mol), HF/CIS ($\Delta E = 15.7$ kcal/mol), and CASSCF ($\Delta E = 23.8$ kcal/mol) predict the formation of a TICT state in the gas phase as a highly endothermic reaction. This is in agreement with experimental data by Polimeno et al.[51] ($\Delta H = 11$ kcal/mol) and Wermuth[48] ($\Delta H = 8$ kcal/mol), but the actual values are far too high as compared with experimental data. Also the ab initio CISDT study by Kato and co-workers[63] yielded an increase in the S_1 state energy of ca. 11 kcal/mol for the twisted conformation relative to the planar geometry. As mentioned earlier (see Section 4), the good agreement between experimental data and the calculations by Kato simply results from an energy shift.

Both the CASPT2 and DFT/CI results have yielded reliable estimates for the characterization of the absorption and the TICT state emission energies, and reliable results are therefore expected for the description of the energies on the S_1 hypersurface. The energy differences, as calculated with these methods, show a slightly exothermic reaction for the formation of the TICT state between -0.88 kcal/mol for the CASPT2 and -2.0 kcal/mol for the DFT/MRCI(BHLYP)/VDZP calculations. If we extrapolate these numbers to the hypothetical HF/CIS-optimized geometry, which yields a less favorable TICT formation, we predict the evolution $L_b \rightarrow$TICT as a slightly endothermic process of ca. 0 to 3 kcal/mol. The $L_b \rightarrow$TICT reaction also becomes endotherm with $\Delta H \approx 8$kcal/mol according to the results by Sobolewski et al.[28] and Sudholt et al.[76] In this work, both the first and second excited state have been optimized, which only has been possible by adopting symmetry restrictions for both excited states. Thus, one cannot directly compare these CASPT2 energies, on the basis of HF/CIS-optimized geometries, with our results taking into account the different assumptions. The TDDFT results again predict a stabilization of the TICT state, which is far too large ($\Delta H = -20.9$ kcal/mol). A comparable TDDFT study by Cammi et al.[74] also yields an unrealistic exothermic reaction $L_b \rightarrow$TICT of about -20 kcal/mol.

6. Conclusion

With the example of spectra and excited-state electron-transfer reaction of DMABN, we have tested and compared many high-level quantum-chemical methods and can draw the following conclusions.

1. Both sophisticated semiempirical and first-principle methods using a basis set with polarization functions are feasible optimization methods for a correct reproduction of the ground-state structures.

2. Optimized ground-state geometries can be used for calculation of absorption energies but optimization of the first excited state is essential for computation of emission energies. The significance of this seemingly obvious statement needs to be emphasized because ground-state geometries are frequently (but falsely or, at best, very approximately) used to calculate emission energies in the literature.

3. Both the AM1/CISD- and HF/CIS-optimized geometries yield reliable results for absorption and emission energies. The results with the HF/CIS-optimized structures are somewhat superior but, because of the incorrect state ordering and close proximity of the L_a and L_b states in this method, only the lowest excited state of a given symmetry can be optimized, because root flipping occurs otherwise.

4. Experimental spectroscopic properties are best reproduced by using the CASPT2 and DFT/MRCI methodologies. Energies are calculated completely wrong by using the HF/CIS, CASSCF, and TDDFT methods; but, in contrast to HF/CIS, CASSCF dipole moments are in fair agreement with experimental data. With TDDFT, no excited-state dipole moments can be calculated. Semiempirical AM1 and DFT/SCI energies are acceptable, but the computed dipole moments clearly deviate from experimental data.

5. Due to point 3 above, the evolution in energy on the first excited-state hypersurface can only be evaluated by using AM1/CISD geometries. Experimentally, an endothermic reaction of 8−11 kcal/mol has been observed from the planar L_b to the TICT state in the gas phase. AM1/CISD, HF/CIS, and CASSCF all calculate an endothermic reaction profile in agreement with experimental data but strongly overestimate the increase in energy. On the other hand, TDDFT calculates a strongly exothermic reaction ($-\Delta H > 20$ kcal/mol). CASPT2 and all DFT/CI methodologies calculate a slightly exothermic reaction, which possibly might become slightly endothermic for HF/CIS geometries.

References and Notes

(1) For a review, see e.g. Davidson, E. R. Ed. *Chem. Rev.* **1991,** *91*, 649.
(2) Foresman, J. B.; Head-Gordon, M.; Pople, J. A.; Frisch, M. J. *J. Phys. Chem.* **1992,** *96*, 135.
(3) Foresman, J. B.; Schlegel, H. B. In *Recent Experimental and Computational Advances in Molecular Spectroscopy*; Fausto, R., Ed.; Kluwer Academic Publishers: Norwell, MA, 1993; p 11.
(4) See e.g. Roos, B. O. In *Ab Initio Methods in Quantum Chemistry II*; Lawley, K. P., Ed.; J. Wiley & Sons Ltd.: New York, 1987; p 399.
(5) Andersson, K.; Malmqvist, P.-Å; Roos, B. O.; Sadlej, A. J.; Wolinski, K. *J. Phys. Chem.* **1990,** *94*, 5483.
(6) Andersson, K.; Malmqvist, P.- Å; Roos, B. O. *J. Chem. Phys.* **1992,** *92*, 1218.
(7) Bauernschmitt, R.; Häser, M.; Treutler, O.; Ahlrichs, R. *Chem. Phys. Lett.* **1997,** *264*, 573.
(8) Stratman, R. E.; Scuseria, G. E.; Frisch, M. J. *J. Chem. Phys.* **1998,** *109*, 8218.
(9) Grimme, S. *Chem. Phys. Lett.* **1996,** *259*, 128.
(10) Grimme, S.; Maletzke, S. *J. Chem. Phys.* **1999,** *111*, 5645.
(11) Van Caillie, C., Amos, R. D., *Chem. Phys. Lett.* **2000,** *317*, 159.
(12) Clark, T. *J. Mol. Struct. THEOCHEM* **2000,** *530*, 1.
(13) Ridley, J.; Zerner, M. *Theor. Chim. Acta* **1972,** *32*, 111.
(14) Lippert, E.; Lüder, W.; Moll, F.; Nägele, W.; Boos, H.; Prigge, H.; Seibold-Blankenstein, I. *Angew. Chem.* **1961,** *21*, 695.
(15) Schuddeboom, W.; Jonker, S. J.; Warman, J. M.; Leinhos, U.; Kühnle, W.; Zachariasse, K. A. *J. Phys. Chem.* **1992,** *96*, 10809.
(16) Lommatzsch, U.; Gerlach, A.; Lahmann, Ch.; Brutschy, B. *J. Phys. Chem. A* **1998,** *102*, 6421.
(17) Grabowski, Z. R.; Rotkiewicz, K.; Siemiarczuk, A.; Cowley, D. J.; Baumann, W. *Nouv. J. Chim.* **1979,** *3*, 443.
(18) Rettig, W. *Angew. Chem., Int. Ed. Engl.* **1986,** *25*, 971.
(19) Rettig, W. *Top. Curr. Chem.* **1994**, *169*, 253.
(20) Zachariasse, K. A.; von der Haar, Th.; Hebecker, A.; Leinhos, U.; Kühnle, W. *Pure Appl. Chem.* **1993,** *65*, 1745.
(21) Zachariasse, K. A. *Chem. Phys. Lett.* **2000,** *320*, 8.
(22) Rauhut, G.; Alex, A.; Chandrasekhar, J.; Steinke, T.; Sauer, W.; Beck, B.; Hutter, M.; Gedeck, P.; Clark, T. *VAMP7.0*; Oxford Molecular Ltd.: Oxford, 1998.
(23) Becke, A. D. *J. Chem. Phys.* **1993,** *98*, 5648.
(24) Frisch, M. J.; Trucks, G. W.; Schlegel, H. B.; Scuseria, G. E.; Robb, M. A.; Cheeseman, J. R.; Zakrzewski, V. G.; Montgomery, J. A., Jr.; Stratmann, R. E.; Burant, J. C.; Dapprich, S.; Millam, J. M.; Daniels, A. D.; Kudin, K. N.; Strain, M. C.; Farkas, O.; Tomasi, J.; Barone, V.; Cossi, M.; Cammi, R.; Mennucci, B.; Pomelli, C.; Adamo, C.; Clifford, S.; Ochterski, J.; Petersson, G. A.; Ayala, P. Y.; Cui, Q.; Morokuma, K.; Malick, D. K.; Rabuck, A. D.; Raghavachari, K.; Foresman, J. B.; Cioslowski, J.; Ortiz, J. V.; Stefanov, B. B.; Liu, G.; Liashenko, A.; Piskorz, P.; Komaromi, I.; Gomperts, R.; Martin, R. L.; Fox, D. J.; Keith, T.; Al-Laham, M. A.; Peng, C. Y.; Nanayakkara, A.; Gonzalez, C.; Challacombe, M.; Gill, P. M. W.; Johnson, B.; Chen, W.; Wong, M. W.; Andres, J. L.; Gonzalez, C.; Head-Gordon, M.; Replogle, E. S.; Pople, J. A. *Gaussian 98*, Revision A.6; Gaussian, Inc.: Pittsburgh, PA, 1998.
(25) Hehre, W. J.; Ditchfield, R.; Pople, J. A. *J. Chem. Phys.* **1972,** *56*, 2257.
(26) Hariharan, P. C.; Pople, J. A. *Theor. Chim. Acta* **1973,** *28*, 213.
(27) Frisch, M. J.; Trucks, G. W.; Schlegel, H. B.; Gill, P. M. W.; Johnson, B. G.; Robb, M. A.; Cheeseman, J. R.; Keith, T.; Petersson, G. A.; Montgomery, J. A.; Raghavachari, K.; Al-Laham, M. A.; Zakrzewski, V. G.; Ortiz, J. V.; Foresman, J. B.; Cioslowski, J.; Stefanov, B. B.;

Nanayakkara, A.; Challacombe, M.; Peng, C. Y.; Ayala, P. Y.; Chen, W.; Wong, M. W.; Andres, J. L.; Replogle, E. S.; Gomperts, R.; Martin, R. L.; Fox, D. J.; Binkley, J. S.; Defrees, D. J.; Baker, J.; Stewart, J. P.; Head-Gordon, M.; Gonzalez, C.; Pople, J. A. *Gaussian 94*, Revisions B.3 and D.4; Gaussian Inc.: Pittsburgh, PA, 1995.

(28) Sobolewski, A. L.; Sudholt, W.; Domcke, W. *J. Phys. Chem. A* **1998,** *102*, 2716.

(29) Sudholt, W.; Sobolewski, A. L.; Domcke, W. *Chem. Phys.* **1999,** *240*, 9.

(30) Andersson, K.; Roos, B. O. In *Modern Electronic Structure Theory*; Yarkony, D. R., Ed.; World Scientific Publishing Co.: Singapore, 1995; Vol. 1, p 55.

(31) Malmqvist, P.-Å.; Roos, B. O. *Chem. Phys. Lett.* **1989,** *155*, 189.

(32) Widmark, P.-O.; Malmqvist, P.-Å.; Roos, B. O. *Theor. Chim. Acta* **1990,** *77*, 291.

(33) Andersson, K.; Blomberg, M. R. A.; Fülscher, M. P.; Karlström, G.; Lindh, R.; Malmqvist, P.-Å.; Neogrády, P.; Olsen, J.; Roos, B. O.; Sadlej, A.-J.; Schütz, M.; Seijo, L.; Serrano-Andrés, L.; Siegbahn, P. E.-M.; Widmark, P.-O. *MOLCAS*, Version 4.1; Lund University: Sweden, 1997.

(34) Ahlrichs R, Bär M, Häser M, Horn H, Kölmel C. *Chem. Phys. Lett.* **1989,** *162*, 165.

(35) Treutler O, Ahlrichs R. *J. Chem. Phys.* **1995,** *102*, 346.

(36) Becke A. D. *J. Chem. Phys.* **1993,** *98*, 1372.

(37) Stephens, P. J.; Devlin, F. J.; Chabalowski, C. F.; Frisch, M. J. *J. Phys. Chem.* **1994,** *98*, 11623.

(38) Dunning TH, Hay PJ. In *Modern Theoretical Chemistry*; Schaefer H. F., III., Ed.; Plenum Press: New York, 1977; Vol. 3.

(39) Schäfer, A.; Horn, H.; Ahlrichs, R. *Chem. Phys.* **1992,** *97*, 2571.

(40) Gibson, E. M.; Jones, A. C.; Philips, D. *Chem. Phys. Lett.* **1988,** *146*, 270.

(41) Heine, A.; Herbst-Irmer, R.; Stalke, D.; Kühnle, W.; Zachariasse, K. A. *Acta Crystallogr.* **1994,** *B50*, 363.

(42) Kajimoto, O.; Yokoyama, H.; Ooshima, Y.; Endo, Y. *Chem. Phys. Lett.* **1991,** *179*, 455.

(43) Jameson, G. B.; Sheikh-Ali, B. M.; Weiss, R. G. *Acta Crystallogr.* **1994,** *B50*, 703.

(44) Mackenzie, R. M.; MacNicol, D. C. *J. Chem. Soc., Chem. Commun.* **1970,** 1299.

(45) Bulliard, Ch.; Allan, M.; Wirtz, G.; Haselbach, E.; Zachariasse, K. A.; Detzer, N.; Grimme, S. *J. Phys. Chem. A* **1999,** *103*, 7766.

(46) Grassian, V. H.; Warren, J. A.; Bernstein, E. R.; Secor, H. V. *J. Phys. Chem.* **1989,** *90*, 420.

(47) Pérez Salgado, F.; Herbich, J.; Kunst, A. G. M.; Rettschnick, R. P. H.; *J. Phys. Chem. A* **1999,** *103*, 3184.

(48) Wermuth, G. *Z. Naturforsch.* **1983,** *38a*, 641.

(49) Rettig, W.; Wermuth, G.; Lippert, E. *Ber. Bunsen-Ges. Phys. Chem.* **1979,** *83*, 692.

(50) Rettig, W. *J. Luminesc.* **1981,** *26*, 21.

(51) Polimeno, A.; Barbon, A.; Nordio, P. L.; Rettig, W. *J. Phys. Chem.* **1994,** *98*, 12158.

(52) Rettig, W.; Braun, D.; Suppan, P.; Vauthey, E.; Rotkiewicz, K.; Luboradzki, R.; Suwinska, K. *J. Phys. Chem.* **1993,** *97*, 13500.

(53) Rotkiewicz, K.; Grabowski, Z. R.; Krówczynski, A.; Kühnle, W. *J. Luminesc.* **1976,** *12/13*, 877.

(54) Kwok, W. M.; Ma, C.; Matousek, P.; Parker, A. W.; Phillips, D.; Toner, W. T.; Towrie, M. *Chem. Phys. Lett.* **2000,** *322*, 395.

(55) Kwok, W. M.; Ma, C.; Matousek, P.; Parker, A. W.; Phillips, D.; Toner, W. T.; Towrie, M.; Umapathy, S. *J. Phys. Chem. A* **2001,** *105*, 984.

(56) Okamoto, H.; Inishi, H.; Nakamura, Y.; Khotani, S.; Nakagaki, R. *Chem. Phys.* **2000,** *260*, 193.

(57) Okamoto, H.; Inishi, H.; Nakamura, Y.; Kohtani, S.; Nagagaki, R. *J. Phys. Chem. A* **2001,** *105*, 4182.

(58) Purkayastha, P.; Bhattacharyya, P. K.; Bera, S. C.; Chattopadhyay, N. *Phys. Chem. Chem. Phys.* **1999,** *1*, 3253.

(59) Broo, A.; Zerner, M. C. *Theor. Chim. Acta* **1995,** *90*, 383.

(60) LaFemina, J. P.; Duke, C. B.; Paton, A. *J. Chem. Phys.* **1987,** *87*, 2151.

(61) Gorse, A.-D.; Pesquer, M. *J. Mol. Struct. THEOCHEM* **1993,** *281*, 21.

(62) Parusel, A. B. J.; Köhler, G.; Grimme, S. *J. Phys. Chem. A* **1998,** *102*, 6297.

(63) Kato S.; Amatatsu, Y. *J. Chem. Phys.* **1990,** *92*, 7241.

(64) Lommatzsch, U.; Brutschy, B. *Chem. Phys.* **1998,** *234*, 35.

(65) Soujanya, T.; Saroja, G.; Samanta, A. *Chem. Phys. Lett.* **1995,** *236*, 503.

(66) Gedeck, P.; Schneider, S. *J. Photochem. Photobiol. A: Chem.* **1997,** *105*, 165.

(67) Gorse, A.-D.; Pesquer, M. *J. Phys. Chem.* **1995,** *99*, 4039.

(68) Dreyer, J.; Kummrow, A. *J. Am. Chem. Soc.* **2000,** *122*, 2577.

(69) Mennucci, B.; Toniolo, A.; Tomasi, J. *J. Am. Chem. Soc.* **2000,** *122*, 10621.

(70) Scholes, G. D.; Philips, D.; Gould, I. R. *Chem. Phys. Lett.* **1997,** *266*, 521.

(71) Chudoba, C.; Kummrow, A.; Dreyer, J.; Stenger, J.; Nibbelring, E. T. J.; Elsaesser, T.; Zachariasse, K. A. *Chem. Phys. Lett.* **1999,** *309*, 357.

(72) Serrano-Andrés, L.; Merchán, M.; Roos, B. O.; Lindh, R. *J. Am. Chem. Soc.* **1995,** *117*, 3189.

(73) Kumrow, A.; Dreyer, J.; Chudoba, C.; Stenger, J.; Nibbering, E. T. A.; Elsaesser, T. *J. Chin. Chem. Soc.* **2000,** *47*, 721.

(74) Cammi, R.; Mennucci, B.; Tomasi, J. *J. Phys. Chem. A* **2000,** *104*, 5631.

(75) Sobolewski, A. L.; Domcke, W. *Chem. Phys. Lett.* **1996,** *259*, 119.

(76) Sudholt, W.; Staib, A.; Sobolewski, A. L.; Domcke, W. *Phys. Chem. Chem. Phys.* **2000,** *2*, 4341.

(77) Parusel, A. B. J. *Phys. Chem. Chem. Phys.* **2000,** *2*, 5545.

(78) López-Tocón, I.; Della Valle, R. G.; Becucci, M.; Castellucci, E.; Otero, J. C. *Chem. Phys. Lett.* **2000,** *327*, 45.

(79) Scholes, G. D.; Gould, I. R.; Parker, A. W.; Phillips, D. *Chem. Phys.* **1998,** *234*, 21.

(80) Rettig, W.; Zietz, B. *Chem. Phys. Lett.* **2000,** *317*, 187.

(81) Baumann, W.; Bischof, H.; Fröhling, J.-C.; Brittinger, C.; Rettig, W.; Rotkiewicz, K. *J. Photochem. Photobiol. A: Chem.* **1992,** *64*, 49.

(82) Rechthaler, K.; Parusel, A. B. J., unpublished results.